Title
Comparison of particulate-matter emissions from liquid-fueled pool fires and fire whirls

Authors
Hariharan, Sriram Bharath
Farahani, Hamed Farmahini
Rangwala, Ali S
et al.

Publication Date
2021-05-01

DOI
10.1016/j.combustflame.2020.12.033

Peer reviewed

Comparison of Particulate Emissions from Liquid-Fueled Pool Fires and Fire Whirls at Different Length Scales

Sriram Bharath Hariharan[a,b], Hamed Farmahini Farahani[b,c], Ali S. Rangwala[c], Joseph L. Dowling[b], Elaine S. Oran[d], Michael J. Gollner[a,b,*]

[a] *Department of Mechanical Engineering, University of California, Berkeley, CA*
[b] *Department of Fire Protection Engineering, University of Maryland, College Park, MD*
[c] *Fire Protection Engineering, Worcester Polytechnic Institute, MA*
[d] *Department of Aerospace Engineering, Texas A&M University, College Station, TX*

Abstract

In-situ burning (ISB) is one of the most effective means of removing oil spilled over open water. While current ISB practices can eliminate a large fraction of the spilled oil, they still result in significant airborne emissions of particulate matter. ISBs are classified as large, free-buoyant pool fires, from which black smoke consisting of particulate matter (PM, soot) emanates as a plume. An experimental investigation of soot emissions from pool fires (PF) and fire whirls (FW) was conducted using liquid hydrocarbon fuels, n-heptane and Alaska North Slope (ANS) crude oil, in fuel pools $10 - 70$ cm in diameter. Burning attributes such as burning rate, fuel-consumption efficiency, and emissions of PM, unburned hydrocarbons, carbon dioxide, and oxygen consumption were measured. For both fuels and all pool diameters, compared to PFs, FWs consumed fuel at a higher rate, had lower post-combustion residual mass and PM emission rates. Collectively, these resulted in consistently lower PM emission factors (EF_{PM}) for FWs at all scales. For FWs, EF_{PM} decreased linearly with a nondimensional quantity defined as the ratio of inverse Rossby number to nondimensional heat-release rate. These results show that the addition of ambient circulation to free-burning PFs to form FWs can increase burning efficiency, reducing both burning duration and EF_{PM} across length scales. The reduction in EF_{PM} with increasing influence of circulation is attributed to a feedback loop of higher temperatures, heat feedback, burning rate and air-entrainment velocity, which in turn contributes to maintaining the structure of a FW. Boilover was observed for fires formed with ANS crude oil at the 70 cm scale, although the overall EF_{PM} was not affected significantly. This investigation presents a foundation to evaluate the detailed mechanisms further, such that appropriate configurations can be developed help minimize the environmental impact of ISBs.

Keywords: *in-situ* burning, emissions, particulate matter, emission factor, fire whirl

*corresponding author
Email address: mgollner@berkeley.edu (Michael J. Gollner)

Nomenclature

Abbreviations

ANS	Alaska North Slope
EF	emission factor
FW	fire whirl
PF	pool fire
ISB	in-situ burning
OF	oxidation factor
PM	particulate matter
TC	thermocouple
UHC	unburned hydrocarbons

Symbols

A_{pool}	area of fuel pool
C	concentration of emission species
c_p	specific heat of air
C_w	heat capacity of water
D	pool diameter
Fr	Froude number
g	gravitational acceleration
Gr	Grashof number
Δh_c	lower heating value of fuel
H_f	flame height
m_w	mass of water sublayer
$\dot{m}$	burning rate
$\dot{m}''$	average mass flux of fuel
M	mass of emission species
$\dot{q}''$	heat-flux feedback
q_f^*	nondimensional heat flux
$\dot{Q}$	heat-release rate
$\dot{Q}^*$	nondimensional heat-release rate
Ri	Richardson number
Ro	Rossby number
S	side length of fire-whirl setup
t_b	burning duration
ΔT	excess temperature at the flame
ΔT_w	rise in temperature of water sublayer
U_θ	tangential velocity
$\dot{V}$	volumetric exhaust flow rate
w_f	flame width
W	gap width

Greek symbols

β	ideal gas expansion coefficient
η_b	burning efficiency
η_{fuel}	fuel-consumption efficiency
ν	kinematic viscosity
Γ	circulation
ρ_b	air density at 1300 K

1. Introduction

1.1. Oil spills and marine pollution

Marine activities, such as oil exploration and extraction, can result in accidental onshore or offshore oil spills. Such oil spills pose a serious threat to surrounding populations [1], response workers [2], and ecosystems [3, 4]. In the event of a spill, an efficient, effective, and robust treatment technique is crucial to mitigate its impact.

In-situ burning (ISB) is one of the most reliable and effective oil spill-treatment techniques [5, 6], particularly in remote regions, harsh climates, or where the size of the accident makes it impossible for immediate mechanical recovery or dispersant techniques to be used. It has been suggested, through laboratory and meso-scale testing of *in-situ* crude oil combustion, that the composition and concentration of emissions from ISB may be an acceptable trade-off in relation to inshore and offshore contamination, its environmental consequences and cleanup costs [5, 7]. In some cases, ISBs have been shown to eliminate at least 90% of the released liquid oil [8, 9]. Thus, ISB remains a fast and portable method of treating oil spills, which is especially important as 70% of the untreated oil spills may emulsify during the first 24 hours [10].

Previous studies quantified emission factors of gaseous species emitted from burning gaseous, liquid, solid fuels [11, 12] and vegetative fuels relevant to wildland fires [13, 14, 15]. Common emission species of interest are particulate matter (PM, soot), CO, CO_2, polycyclic aromatic hydrocarbons (PAHs), and volatile organic compounds (VOCs). Recent work on pool-fire burning of gaseous and liquid fuels [12] quantified these emissions by periodic sampling in the fire plume, assuming that the products of combustion CO_2, CO, methane and unburned hydrocarbons (UHC) were distributed uniformly in the plume, and defining emission factors for each species based on the mass of carbon burned.

Large pool fires such as ISBs are oxygen-starved due to limited air entrainment into the central flame core above the fuel surface [16, 17]. Additionally, crude oil contains a high fraction of heavy hydrocarbons [18]. Hence, ISB pool fires are prone to emitting large quantities of soot, seen as black smoke emanating from ISBs. The emission of soot (PM) is one of the major operational limits of current ISB practices as high concentrations can cause health concerns for populations in downwind regions. Such fires are also nonpremixed flames, where lower oxygen concentrations, high temperatures and long residence times are favorable for soot inception and growth [19].

Increasing burning efficiency and reducing PM emissions requires combustion to take place with higher oxygen concentrations, better mixing and shorter residence times. Re-

placing pool fires (PF) with fire whirls (FW) could provide these conditions. Applications such as the cleanup of spilled oil over the ocean through ISB and waste incinerators for complex fuels present the motivations to study and evaluate the differences in emissions between PFs and FWs.

1.2. Fire whirls

The addition of swirling flow in a combustor improves flame stability, enhances combustion efficiency and reduces emissions [20]. In swirl combustors using a jet flame, reduction in emissions depends on improving fuel-air mixing by increasing the turbulence intensity and operating in the fuel-lean regime [21, 22]. While there are similarities between swirl combustion and FWs, they differ in the manner of air entrainment. In swirl combustion, air is usually premixed with fuel and injected through a central fuel port or spray injector with considerable axial momentum. In FWs, however, air entrainment primarily occurs in the radial direction at the bottom surface boundary over which a FW is formed, and there is negligible axial momentum from air entrainment. The result is that combustion occurs mostly as a nonpremixed flame [23] in a cylindrical structure that is described by the Burger's vortex [24]. In contrast to swirl combustion, turbulence is generally suppressed in FWs [25]. The fundamental question that needs to be answered to evaluate the potential for using FWs in ISBs is – when compared to PFs, do FWs emit lower quantities of airborne soot?

The objective of this work is to determine whether burning a pool of liquid fuel as a FW can result in lower PM emissions than when burning as a PF. PFs and FWs were formed at different length scales, with liquid-fuel pools 10, 20, 30 and 70 cm in diameter. Burning characteristics such as burning rate, fuel-consumption efficiency, emissions of PM, unburned hydrocarbons (UHC), CO_2, heat feedback to the fuel pool, and emission factors for each species were used to compare the two regimes. Finally, scaling parameters influencing a reduction in PM emissions in FWs are discussed, and a preliminary explanation of the factors controlling this behavior is presented.

2. Experimental methods

2.1. Apparatus

A fixed-frame, four-wall fire whirl configuration [26, 27] was used to form FWs at all pool diameters (see Figure 1A). In this configuration, the buoyancy of the fire plume inside the enclosure causes air to be entrained through the four gaps, generating the ambient swirl required to form FWs. Stable and reliable FW formation was observed when the ratio of the width of each gap (W) to the width of the side wall of the enclosure (S) was fixed at $W/S = 1/4$. The walls were removed for PF experiments. A circular aluminum dish was used to hold the fuel pool, with varying diameters ($D = 10, 20, 30, 70$ cm). The dish was used to hold a water sublayer above which the fuel slick floated, mimicking open-water conditions. The top edge of the dish was flush with the bottom surface of the enclosure. Experiments for $D = [10, 20, 30]$ cm were performed at the University of Maryland, and those at $D = 70$ cm scale were performed at Worcester Polytechnic Institute.

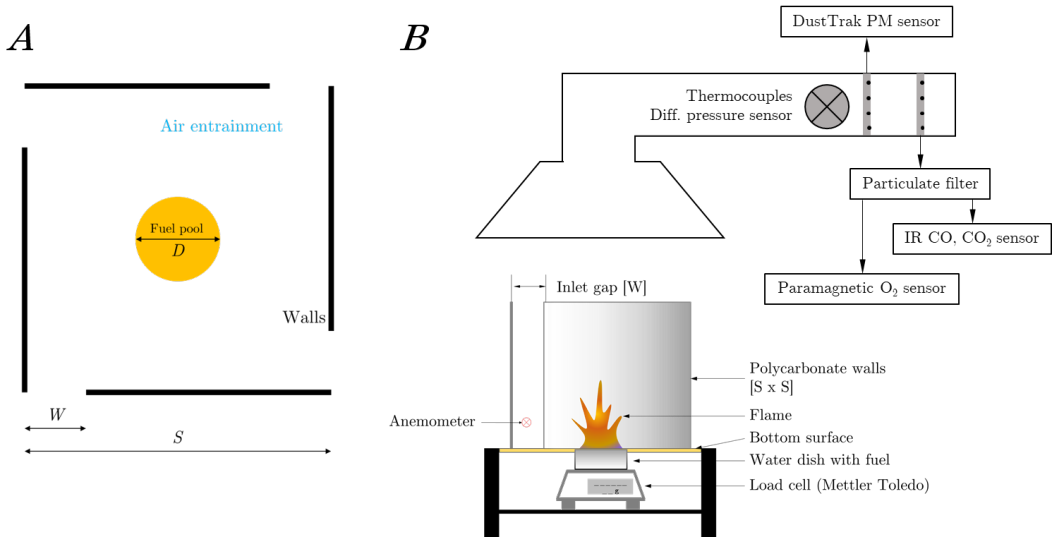

Figure 1: Schematic of experimental setup.

For $D = [10, 20, 30]$ cm, the fuel dish was placed over a load cell to measure instantaneous mass. This data was then used to calculate the mass-loss (burning) rate. Burning rate at $D = 70$ cm was measured as the ratio of total mass of fuel consumed to the burning duration. The residue mass was measured by noting the weight of 3M adsorbent pads before and after collecting the residue. The velocity of air entrainment through the gaps into the enclosure was measured using a Testo 450i vane anemometer positioned at the center of one gap between the enclosure walls. Since the measurement was made at the periphery of the enclosure, the average inlet velocity may be assumed to be in the azimuthal direction and denoted as (U_θ). The different experimental conditions are shown in Table 1.

Boilover is a rapid combustion process that occurs during burning of thin films of heavy hydrocarbon fuel (such as ANS crude oil) which is spread over a water sublayer. This usually occurs during laboratory-scale experiments and an important parameter that controls the onset of boilover is the temperature of the water-fuel interface. To keep this temperature below the boiling point of water and avoid boilover in the $D = [10, 20, 30]$ cm scales, a magentic stirrer was used to mix the water sublayer. For $D = 70$ cm, the thickness of the crude oil slick was increased to 7 mm, and a pump system was used to recirculate water in the sublayer, but boilover could not be avoided. The impact of the onset of boilover on emission factors is discussed in detail in section 4.2.

For $D[10, 20, 30]$ cm scales, the temperature of the water sublayer was measured using four K-type thermocouples (75 μm bead diameter) submerged in the sublayer. The mass of water in the sublayer (m_w) was measured before each experiment, and the total rise in bulk water temperature (ΔT_w) was obtained. Using these, the temporally and spatially averaged heat feedback $(\dot{q}'')$ was calculated as $\dot{q}'' = (m_w C_w \Delta T_w)/(A_{pool} t_b)$, where C_w is the heat capacity of water, A_{pool} is the area of the fuel pool, and t_b is the burning duration. For $D = 70$ cm, a Schmidt-Boelter gauge was positioned in the center of the pool to directly measure the total (convection and radiation) heat feedback.

Table 1: Experimental conditions for PFs and FWs formed using heptane and ANS crude oil.

Pool diameter D [cm]	Gap width W [cm]	Enclosure side length, S [cm]	Enclosure wall height, H [cm]	Fuel volume [ml]	Slick thickness [mm]
10	15	60	60	40	5
20	25	100	100	160	5
30	25	100	100	350	5
70	45	175	240	3000	7

The FW setup was placed under an exhaust suction hood to collect all the combustion products. A schematic of the arrangement is shown in Figure 1B. The exhaust duct was instrumented with two sampling tubes − one connected to a TSI DustTrak 8534 for measuring PM, and the other connected to a California Instruments CAI ZPA NDIR/O_2 gas analyzer with a particulate filter positioned upstream. Three K-type thermocouples, with a bead diameter of 50 μm, were positioned within the duct to measure temperature at the gas-sampling location. Instantaneous flow rate was measured using a Verabar V100 differential pressure sensor installed immediately upstream of the sampling location in the exhaust duct. For the experiments at $D = 70$ cm, a Spectris Servomex 4200 gas analyzer was used to measure the concentration of gaseous species. In all cases, the concentration of CO_2, CO and O_2 was measured in the range 0–10%, 0–1% and 0–25%, respectively. A gravimetric calibration of PM measurements [28] was performed using a 0.8 μm filter operated concurrently in parallel with the DustTrak.

2.2. Calculating emission factors

A two-point reference calibration for CO_2, CO and O_2 was performed for the gas analyzer by using 100% N_2 for the zero value, and a mixture of 0.8% CO, 8% CO_2 and 21% O_2 for the span value. The instantaneous concentration measured for each species and the total volumetric flow rate through the duct were used to calculate the emission rate in units of [mass/time]. The total mass, M, of each species was measured as an integral over time,

$$M\Big[mg\Big] = \dot{V}\Big[\frac{m^3}{s}\Big] \int_0^{t_b} C\Big[\frac{mg}{m^3}\Big] dt\Big[s\Big] \tag{1}$$

where $\dot{V}$ is the volumetric flow rate measured in the exhaust duct, C is the concentration measured by either the gas analyzer or PM sensor, and t_b is the burn duration.

The concentration of unburned hydrocarbons (UHC) was not directly measured. Instead, it was estimated by using the carbon mass balance approach [11], assuming that the emissions were composed of four carbon-containing species, CO_2, CO, PM and UHC. The carbon mass

emitted as UHC was estimated as the difference between carbon mass in the fuel consumed and the total carbon mass measured as CO_2, CO and PM. The carbon mass in heptane and ANS crude oil was 84% and 85.9% [18], respectively. For each of the emitted species, an emission factor was defined as

$$\mathrm{EF}_{\mathrm{species}} = \frac{\text{Mass of carbon in emission species [g or kg]}}{\text{Mass of carbon in fuel consumed [kg]}} \tag{2}$$

based on the carbon mass in the species and carbon mass in burned fuel, similar to previous work [11, 29]. The burning efficiency (η_b) was defined as

$$\eta_b = \frac{\text{Mass of carbon emitted as } CO_2}{\text{Total mass of carbon in } CO_2\text{, CO, PM, UHC}} \tag{3}$$

to compare the relative amount of C emitted as CO_2 to the total mass of C emitted from the fuel as CO_2, CO, UHC and PM. In this way, both η_b and EF are bounded between 0 and 1, and also causes η_b to be numerically equal to EF_{CO_2}. Finally, oxidation factor (OF) was defined for each case as

$$\mathrm{OF} = \frac{\text{Mass of } O_2 \text{ emitted as } CO_2}{\text{Total mass of } O_2 \text{ consumed}} \tag{4}$$

which quantifies the fraction of total oxygen consumed that is emitted as CO_2. An oxidation factor of 1 implies all the O_2 consumed is emitted in the form of CO_2.

3. Results

3.1. Physical Characteristics of PFs and FWs

For each experiment, photographs of PFs and FWs were obtained using a digital camera. Some of these images are shown in *Supplementary Figures 1 and 2*. For PFs, the average flame height, $H_f \in [1, 2]D$. At the base of PFs, the flame width, w_f, is equal to the pool diameter, D. PFs have a conical flame shape as w_f reduces with axial distance. Entrained air along the boundary layer toward a PF causes necking of the flame at the base and initiates Rayleigh-Taylor instabilities [30], which cause the flame sheet to roll up (see *Supplementary Figure 1A*) and fluctuate periodically [31], a phenomenon referred to as "puffing." In contrast to PFs, $H_f \in [3, 6]D$ for FWs, which have a cylindrical shape. FWs also show stronger necking at the base of the flame, resulting in reduced average flame width, $w_f \in [0.5, 1)D$. FWs do not show puffing, which is replaced by a helical instability that causes the flame to wrap around a vortex core [32].

The rate of fuel consumption (burning rate, $\dot{m}$) was measured using instantaneous mass data from the load cell for $D = [10, 20, 30]$ cm. Since the load cell could not be used for the large 70 cm pool, $\dot{m}$ was estimated as the ratio of the total mass of fuel burned to the burn duration. The variation of burning rate with D (Figure 2A) shows that for both heptane and ANS crude oil, $\dot{m}$ is higher for FWs. The experimental variability in the measurement of $\dot{m}$ was negligible, resulting in very small error bars in Figure 2A. For fires formed using

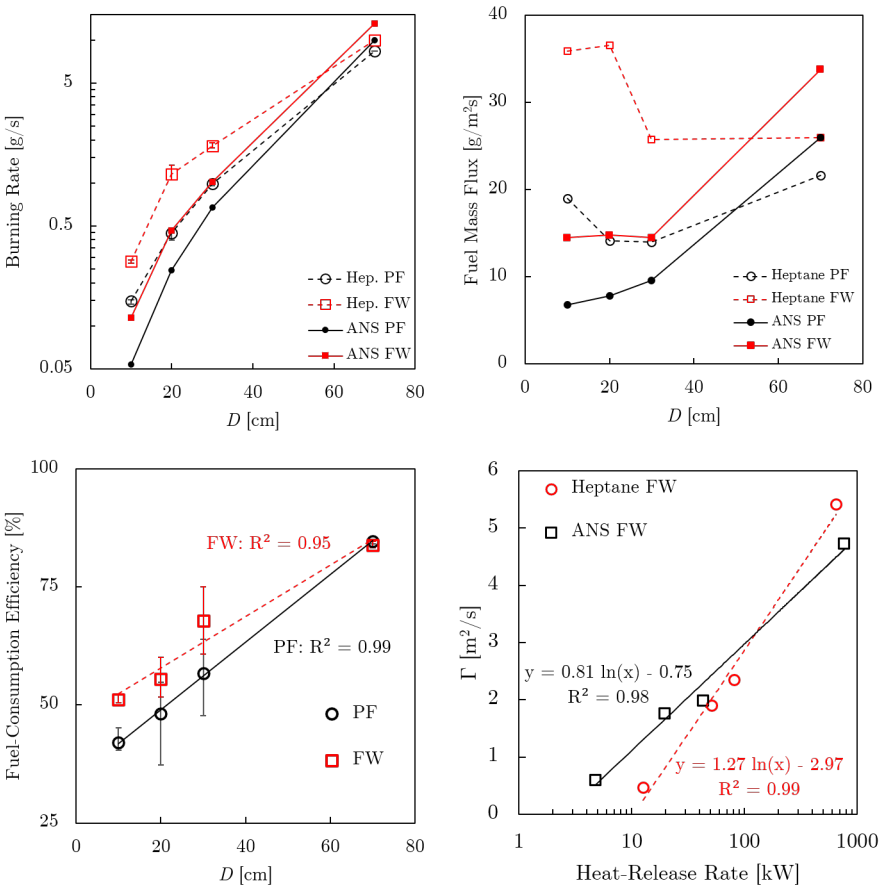

Figure 2: Comparison of (A) $\dot{m}$ and (B) $\dot{m}''$ for PFs and FWs. (C) Variation of η_{fuel} with D for ANS fires. (D) Combinations of $\dot{Q}$ and Γ for the FWs in this study, showing a logarithmic relationship.

each fuel at $D = [10, 20, 30]$ cm, the ratio of burning rate of FWs to PFs is about 2, and this ratio reduceds to about 1.3 at $D = 70$ cm.

Comparing each flame regime individually for $D = [10, 20, 30]$ cm, $\dot{m}$ for heptane fires is larger than that for ANS fires. This trend, however, reverses at $D = 70$ cm, where $\dot{m}$ of ANS is higher than that of heptane. This is also evident in Figure 2B, which shows the variation of fuel mass flux ($\dot{m}''$) for the different conditions. These quantities are tabulated in *Supplementary Table 1.*

Upon extinction of ANS crude oil fires, some residue remained on the water surface. This residue is primarily composed of heavier hydrocarbons and tars in the fuel [18]. Measurable residues were not observed with heptane fuel. For ANS fires, fuel-consumption efficiency (η_{fuel}) was defined as the ratio of fuel mass burned to the total initial mass of the fuel, and is shown in Figure 2C. η_{fuel} is higher for FWs when $D = [10, 20, 30]$ cm, but this difference is negligible at $D = 70$ cm. The sharp rise in $\dot{m}''$ for ANS fires and the negligible difference in η_{fuel} between PFs and FWs at $D = 70$ cm scale are both attributed to boilover (section 4).

3.2. Circulation and heat feedback

The combination of circulation (Γ) and heat-release rate ($\dot{Q}$) defines the state and shape of a FW [33]. Values of Γ and $\dot{Q}$ for the FWs in this study are shown in Figure 2D. The $\dot{Q}$ was estimated as $\dot{Q} = \dot{m}\,\Delta h_c$, where Δh_c is the lower heating value of the fuel, and Γ was estimated as $\Gamma = 4\,S\,U_\theta$. The $\dot{Q}$ of the FWs in this study spans three orders of magnitude, wider than most previous studies. According to the classification by Lei et al. [33], the shapes of the FWs in this study may generally be considered as cylindrical FWs.

The Γ calculated for the FWs in this study is compared to the inverse of the Rossby number in Figure 3A. The quantity Ro^{-1} describes the ratio of azimuthal momentum from circulation to the buoyant (axial) momentum from heat release. Following [34], Ro^{-1} was estimated as $(\Gamma D)/(\dot{m}''/\rho_b)$, where ρ_b is the air density at $T = 1300$ K. While Γ increases continuously with pool diameter, Ro^{-1} increases from the $10-30$ cm scales, but is relatively unchanged between the 30 and 70 cm scales. Both Γ and Ro^{-1} are generally higher for FWs formed using heptane when compared to those formed using ANS crude oil.

The variation of average heat-flux feedback, $\dot{q}''$, with D is shown in Figure 3B. $\dot{q}''$ is higher for FWs at all scales, although the difference is very small in the $10-30$ cm scales. At $D = 70$ cm, however, $\dot{q}''$ for FWs is more than twice that for PFs. Also, for both the flame regimes, the value of $\dot{q}''$ is higher for fires formed with ANS crude oil than those formed with heptane, partly due to the higher concentration of soot particles in the flame (see section 3.3). For FWs, since Γ increases linearly with D, $\dot{q}''$ also increases roughly linearly with Γ (Figure 3C). For each case, nondimensional heat flux was estimated from [35] as $q_f^* = \dot{q}'' \,/\, (\rho_0\, c_p\, \Delta T\, \sqrt{gD})$ and its variation with Γ is shown in Figure 3D. In general, an increase in circulation corresponds to an increase in heat flux feedback to the pool, similar to previous studies [36, 37]. The experimental variation is higher for fires at $D = 70$ cm since these measurements were made directly using a Schmidt-Boelter gauge, whereas experiments in the smaller scales were averaged temporally and spatially, and instantaneous fluctuations are not apparent.

3.3. Emissions

The DustTrak 8534 instrument, used to measure PM concentrations in the exhaust duct, can distinguish two size ranges of PM, PM-2.5 and PM-10, denoting particle sizes below 2.5 μm and 10 μm, respectively. But measurements showed little variation between the concentrations of these particle sizes, indicating most particulates are 2.5 μm in diameter or smaller. Therefore, these measurements are reported as Total PM (TPM) here. During combustion of each regime, measurements were obtained at a frequency of 1 Hz, and the experimental results are shown in 4. Panels (A) and (B) compare heptane fires, and panels (C) and (D) compare ANS fires, with the different line colors indicating individual experiments. PM emission rate data for the other scales are included as *Supplementary Figures 3–5*.

As FWs have a higher burning rate than PFs, the duration of PM emission is lower. The peak emission rate of PM is higher for PFs (250 mg/s for heptane PF, 3000 mg/s for ANS PF) than for FWs (175 mg/s for heptane FW, 2300 mg/s for ANS FW). The instantaneous PM emission rate from ANS fires is an order magnitude higher than that from the heptane

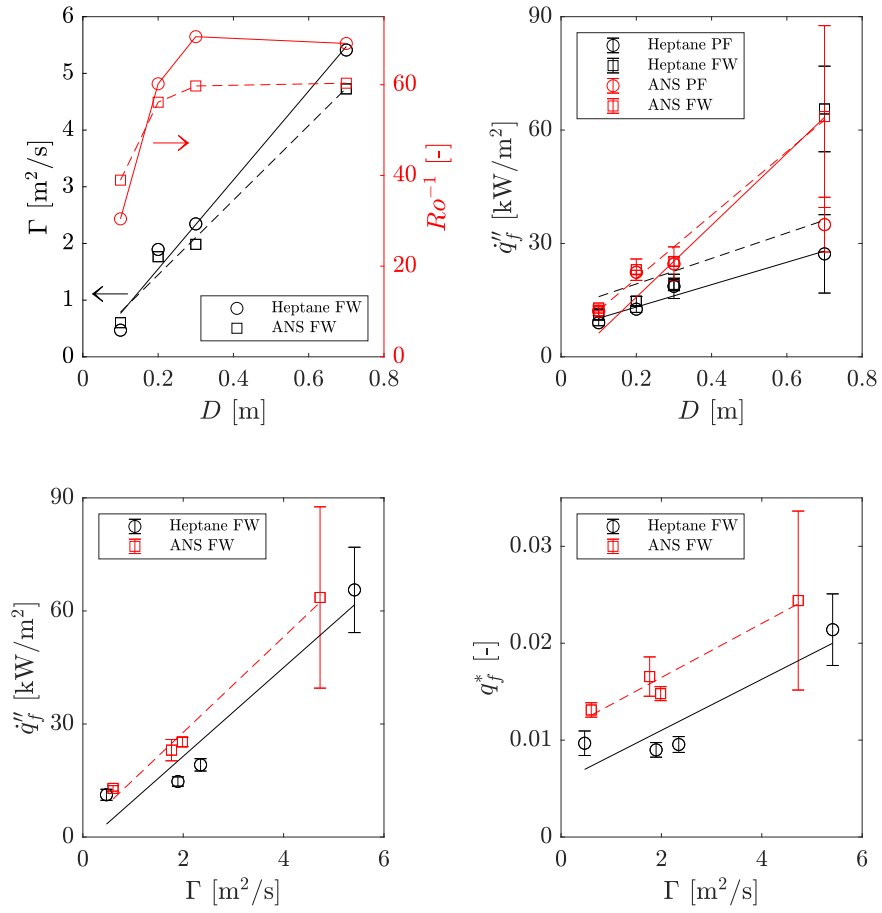

Figure 3: Variation of (A) Γ and Ro^{-1} with D, (B) $\dot{q}''_f$ with D. Panels (C) and (D) show the linear increase in $\dot{q}''_f$ and q^*_f with Γ for FWs. Solid lines indicate linear fits for heptane FWs, and dashed lines indicate those for ANS FWs.

fires. For heptane fires, the peak emission rate is observed roughly around the middle of the burn duration. For ANS fires, however, there is an initial linear increase in the emission rate from ignition, with a sudden spike in the rate, followed by a quick drop towards extinction. The sharp spike in the emission rate (at ∼65 s for ANS FWs, ∼110 s for ANS PFs) is caused by the onset of boilover. Boilover was seen only with the 70 cm ANS crude oil experiments, and hence the sharp rise in PM emission rate was not seen in ANS fires at $D = [10, 20, 30]$ cm.

The PM emission factor, EF_{PM}, calculated according to Equation 2 is presented in Figure 4, which shows that FWs emit a lower mass of PM per unit mass of fuel burned. For all the different fire conditions, the lowest EF_{PM} occurs at $D = 30$ cm. Additionally, for PFs and FWs formed using ANS crude oil, the value of EF_{PM} in the pre-boilover and post-boilover periods are similar to the overall EF (Figure 4F).

The EFs of UHC (EF_{UHC}) and of CO_2 (EF_{CO_2}) are shown in Figure 5. The lowest EF_{UHC} is seen at $D = 20$ cm for both heptane and ANS crude oil. For heptane fires (Figure 5A), EF_{UHC} for FWs is slightly lower than from PFs, and this simultaneously corresponds to slightly higher EF_{CO_2} (Figure 5C). For ANS fires at $D = [10, 70]$ cm, EF_{UHC} is slightly lower for FWs, along with slightly higher EF_{CO_2}. At $D = [20, 30]$ cm, however, FWs show slightly higher EF_{UHC} but lower EF_{CO_2} (Figure 5D). Compared to CO_2 and UHC, CO is found only in trace amounts. EF_{CO} is shown in Figures 5E and 5F. For heptane fires, FWs show lower EF_{CO} than PFs. This is reversed for ANS fires, with FWs showing higher EF_{CO} than PFs.

The EFs discussed above were calculated based on the mass of carbon in the fuel. The EFs determined on the basis of the total fuel mass burned are tabulated for all species in Table 2. EFs calculated by the two methods vary numerically, but show the same trend with D. The mass of UHC emitted was calculated using the molecular weight of propane (C_3H_8) and the estimate of carbon emitted as UHC.

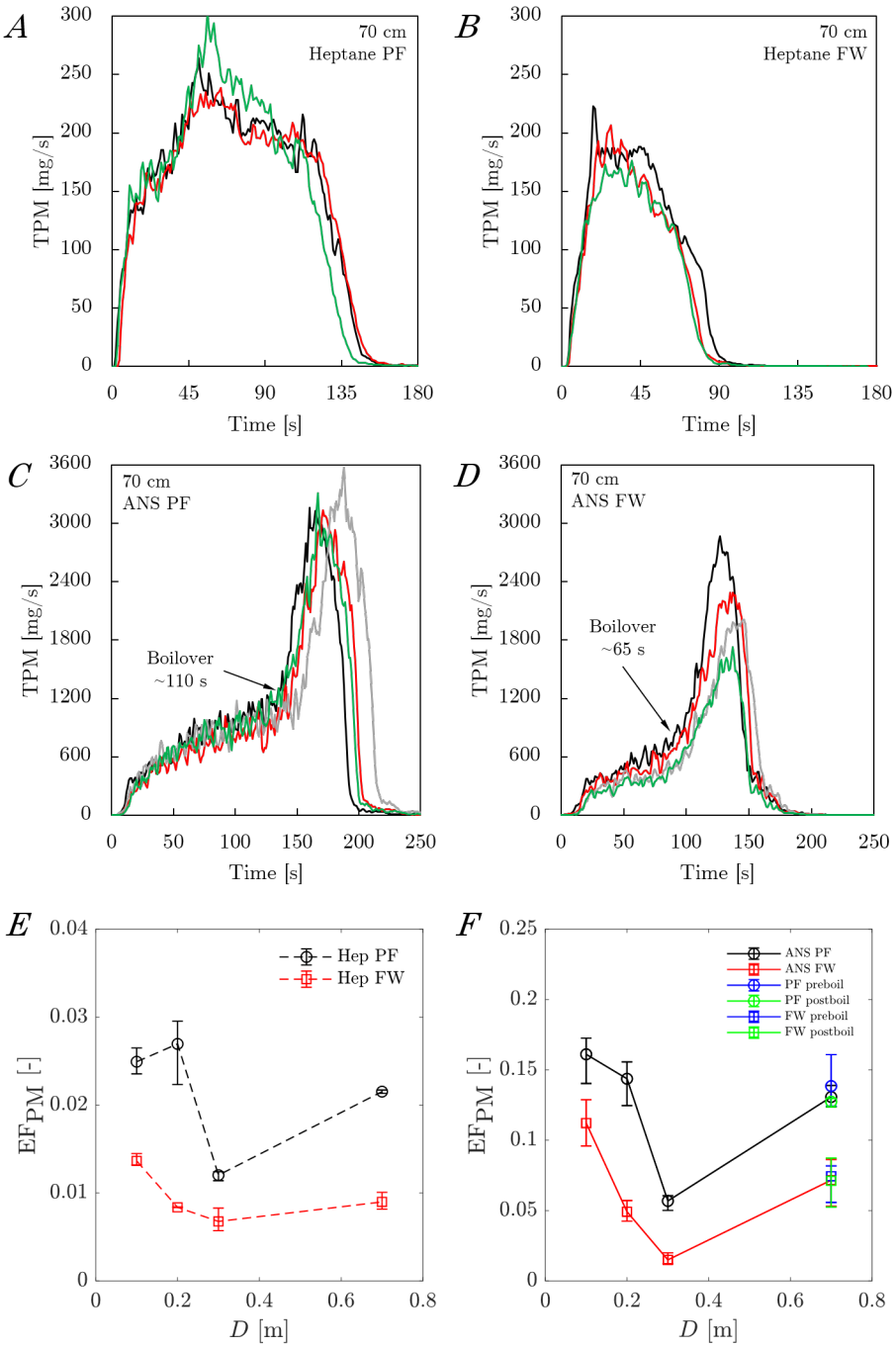

Figure 4: PM emission rate, measured at 1 Hz, as a function of time for heptane fires at $D = 70$ cm are shown in panels (A) and (B). Data for ANS fires at $D = 70$ cm are shown in panels (C) and (D). Boilover is evident in the PM emission rate for both ANS PFs and FWs. $\mathrm{EF_{PM}}$ is shown as a function of D in panels (E) and (F). Panel (F) shows markers for overall $\mathrm{EF_{PM}}$, and those calculated for the pre- and post-boilover periods.

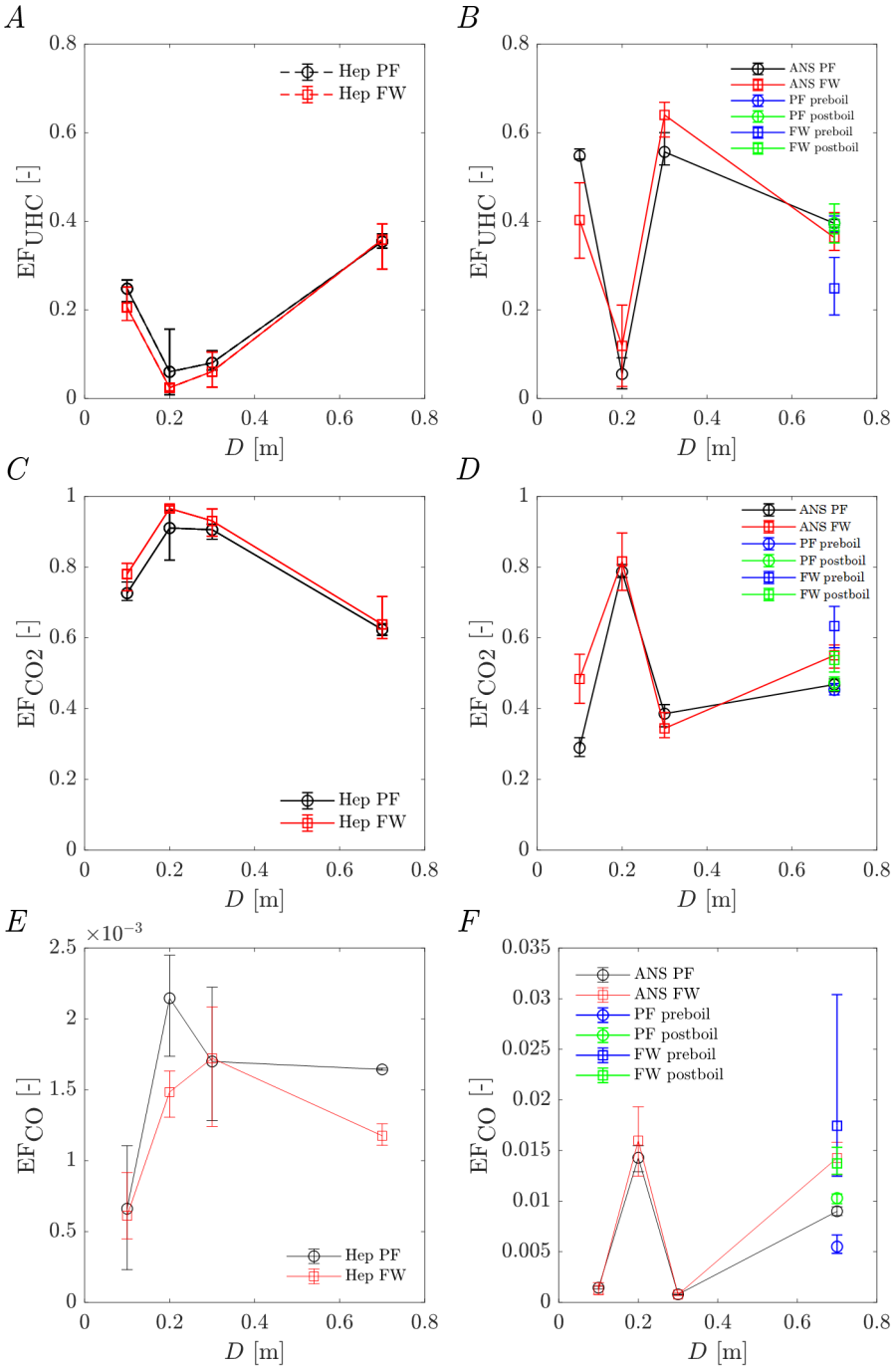

Figure 5: Variation of different EFs with D. $\mathrm{EF_{UHC}}$ is shown in panels (A) and (B), $\mathrm{EF_{CO_2}}$ in panels (C) and (D), and $\mathrm{EF_{CO}}$ in panels (E) and (F). Data for ANS fires at $D = 70$ cm includes markers for the pre- and post-boilover periods.

Table 2: Tabulated values of EF for the different emission species. For each EF, the mean of three experiments is shown for both fuel-mass based and fuel-carbon-mass based estimation methods.

		Emission Factor based on total fuel mass					Emission Factor based on carbon mass in fuel				
	Scale [cm]	EF_{PM} [kg/kg]	EF_{CO_2} [kg/k]g	EF_{CO} [kg/kg]	CF_{O_2} [kg/kg]	EF_{UHC} [kg/kg]	EF_{PM} [kg/kg]	EF_{CO_2} [kg/kg]	EF_{CO} [kg/kg]	CF_{O_2} [kg/kg]	EF_{UHC} [kg/kg]
Heptane Pool Fire	10	0.021	2.238	0.001	3.193	0.254	0.025	0.727	0.001	3.801	0.248
	20	0.023	2.805	0.004	3.236	0.062	0.027	0.911	0.002	3.853	0.060
	30	0.010	2.790	0.003	3.067	0.083	0.012	0.906	0.002	3.651	0.080
	70	0.018	1.921	0.003	2.178	0.364	0.022	0.624	0.002	2.593	0.354
Heptane Fire Whirl	10	0.011	2.403	0.001	2.909	0.211	0.014	0.780	0.001	3.464	0.205
	20	0.007	2.975	0.003	3.237	0.025	0.008	0.966	0.001	3.854	0.024
	30	0.005	2.867	0.003	3.168	0.062	0.007	0.931	0.002	3.772	0.061
	70	0.008	1.965	0.002	2.196	0.369	0.009	0.638	0.001	2.615	0.359
ANS Pool Fire	10	0.148	0.912	0.003	3.426	0.575	0.161	0.290	0.001	3.989	0.548
	20	0.141	2.851	0.032	3.016	0.058	0.144	0.787	0.014	3.511	0.055
	30	0.049	1.215	0.002	1.764	0.584	0.057	0.386	0.001	2.054	0.557
	70	0.113	1.501	0.018	1.629	0.415	0.131	0.468	0.009	1.874	0.395
Pre-boilover	70	0.119	1.426	0.011	0.910	0.416	0.138	0.453	0.006	1.874	0.396
Post-boilover		0.109	1.492	0.021	2.419	0.484	0.127	0.474	0.010	1.874	0.396
ANS Fire Whirl	10	0.097	1.524	0.002	4.112	0.423	0.112	0.484	0.001	4.787	0.403
	20	0.042	2.571	0.032	2.590	0.125	0.049	0.816	0.016	3.016	0.119
	30	0.013	1.037	0.002	1.299	0.672	0.015	0.344	0.001	1.512	0.640
	70	0.062	1.741	0.029	1.997	0.381	0.072	0.551	0.014	2.290	0.363
Pre-boilover	70	0.064	1.995	0.035	0.550	0.261	0.074	0.633	0.017	2.290	0.249
Post-boilover		0.061	1.693	0.028	3.379	0.467	0.071	0.538	0.014	2.290	0.382

4. Discussion

The experimental results presented above show that a pool of liquid fuel when burned as a FW, in comparison to a PF, has a higher burning rate and emits lower peak concentrations of airborne PM. These factors together result in a lower EF_{PM} for FWs. Additionally, when ANS crude oil is used as the fuel, FWs had a higher η_{fuel} since the residual mass upon extinction was lower. A minimum slick thickness of $2 - 2.5$ mm is required to sustain burning over water surfaces [5, 38] due to heat loss to the water surface beneath the fuel. Consequently, the consumption efficiency for a given flame regime and pool diameter is directly proportional to the initial slick thickness since all fires will eventually burn down to the minimum slick thickness.

The behavior of EF_{PM} also shows significant dependence on the fuel type. The EF_{PM} for ANS fires is an order of magnitude higher than those for heptane. Lighter fuels are known to have lower EFs than fuels that are contain high-molecular weight, complex components [11, 12]. For a given flame regime and D, higher values of EF_{PM} are seen for crude oil, a multi-component fuel with long-chain hydrocarbons with complex structures [18].

The addition of swirl to jet flames results in the reduction of emissions from swirl burners [21]. In swirl burners, the reduction in emissions is enabled by enhanced mixing that is caused by increased levels of turbulence intensity, which allows combustion to approach premixed conditions. Turbulence, however, is suppressed in FWs, and this is one of the reasons for elongation of the flame as compared to a PF formed over a pool at the same D [23, 25]. The reduced effect of turbulence is evident in the lower values of the Grashof number (Gr) for PFs (Figure 6). Gr was estimated as $Gr = g\beta\Delta T D^3/\nu^2$, where g is gravitational acceleration, β is the ideal-gas expansion coefficient, ΔT is the excess temperature, and ν is the kinematic viscosity. Gr increases significantly with D, but only the fires at $D = 70$ cm approach the turbulent regime ($Gr > 10^9$) [39]. Thus, the lower value for EF_{PM} for FWs is not explicable based on turbulence or mixing effects.

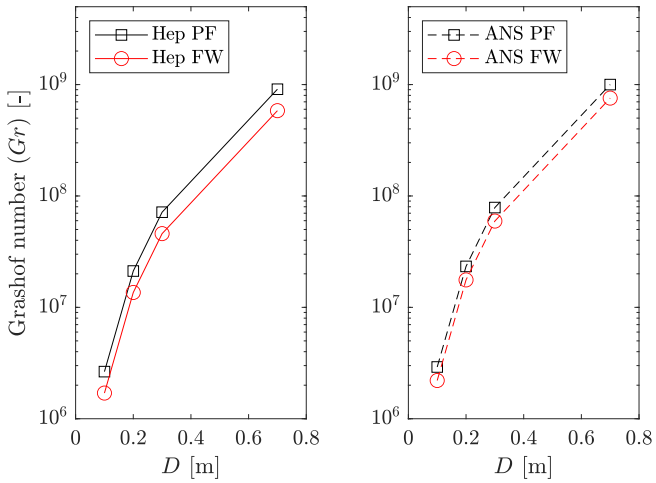

Figure 6: Grashof number (Gr) at different values of D for the different cases.

The values EF_{UHC} and EF_{CO_2} are at least an order of magnitude higher than EF_{PM}, showing that a majority of the carbon in the fuel is emitted in the form of gaseous components, and that only a small fraction is emitted as particulate soot. So, small differences in the values of EF_{UHC} and EF_{CO_2} between the PF and FW regimes can cause significant differences in EF_{PM}. This is evident when comparing Figure 4 (C,D) with Figure 5 – the value of EF_{PM} for FWs is roughly half that of PFs, but the values of EF_{UHC} and EF_{CO_2} are within 10% of each other for the different cases.

In the following section, we focus on the nondimensional quantity, EF_{PM}, and use FW-scaling parameters to provide preliminary explanations of the differences between PFs and FWs that lead to reduced emissions.

4.1. Scaling

In a FW setup with natural entrainment, Γ is intrinsically coupled with $\dot{Q}$ [40]. This is because the buoyancy, that stems from $\dot{Q}$, controls the strength of air entrainment into the enclosure, U_θ, which in turn determines Γ. The effect of circulation on FWs is represented by either the Froude number ($Fr = U_\theta^2/gD$), which is analogous to the Richardson number ($Ri = g\beta\Delta T D/U_\theta^2$), or the inverse Rossby number, Ro^{-1}. Both Fr and Ri represent the competing effects of tangential momentum from ambient circulation and buoyant momentum from heat release. While Ri has previously been used to describe H_f [41], Chuah et al. [34] showed that the effect of circulation on FWs and H_f was better represented by the inverse Rossby number (Ro^{-1}), a nondimensional quantity that is equivalent to Ri. The effect of buoyancy on the FW is represented in the form of a nondimensional heat-release rate, $\dot{Q}^*$, defined for FWs as [42]

$$\dot{Q}^* = \frac{\dot{Q}}{\rho_0 \, \Delta T \sqrt{gD^5}} \tag{5}$$

where ρ_0 is the ambient air density [43], $\dot{Q}$ is the average heat-release rate. The variation of $\dot{Q}^*$ with D is shown in Figure 7A. We now define the ratio ($Ro^{-1}/\,\dot{Q}^*$) to compare the effects of buoyancy and circulation for FWs formed at different length scales. The effect of this ratio on EF_{PM} for heptane and ANS FWs is shown in Figure 7B.

For ANS FWs, Figure 7A shows a linear relationship between EF_{PM} and ($Ro^{-1}/\dot{Q}^*$). EF_{PM} decreases as ($Ro^{-1}/\dot{Q}^*$) increases, indicating that as the effect of circulation increases relative to buoyancy, conditions are favorable for lower PM emissions. The ratio ($Ro^{-1}/\dot{Q}^*$) has a similar effect on EF_{PM} from heptane fires, with the lowest emissions seen at ($Ro^{-1}/\dot{Q}^*$) ≈ 150. Beyond this value, however, there is an increase in EF_{PM} for heptane FWs.

For a given fuel and D, with the increasing effect of circulation, EF_{PM} reduces linearly with ($Ro^{-1}/\dot{Q}^*$), but there exists an upper limit beyond which EF_{PM} rises again. The increase in EF_{PM} for heptane fires beyond this threshold value agrees with previous observations of FW behavior under high values of Γ – above a certain value of ambient Γ, FWs show reduced H_f, increased w_f, and increased soot emissions that are visible as black smoke [44, 45, 33]. Recent experiments conducted by Lei et al. [33] showed that as Γ is increased at

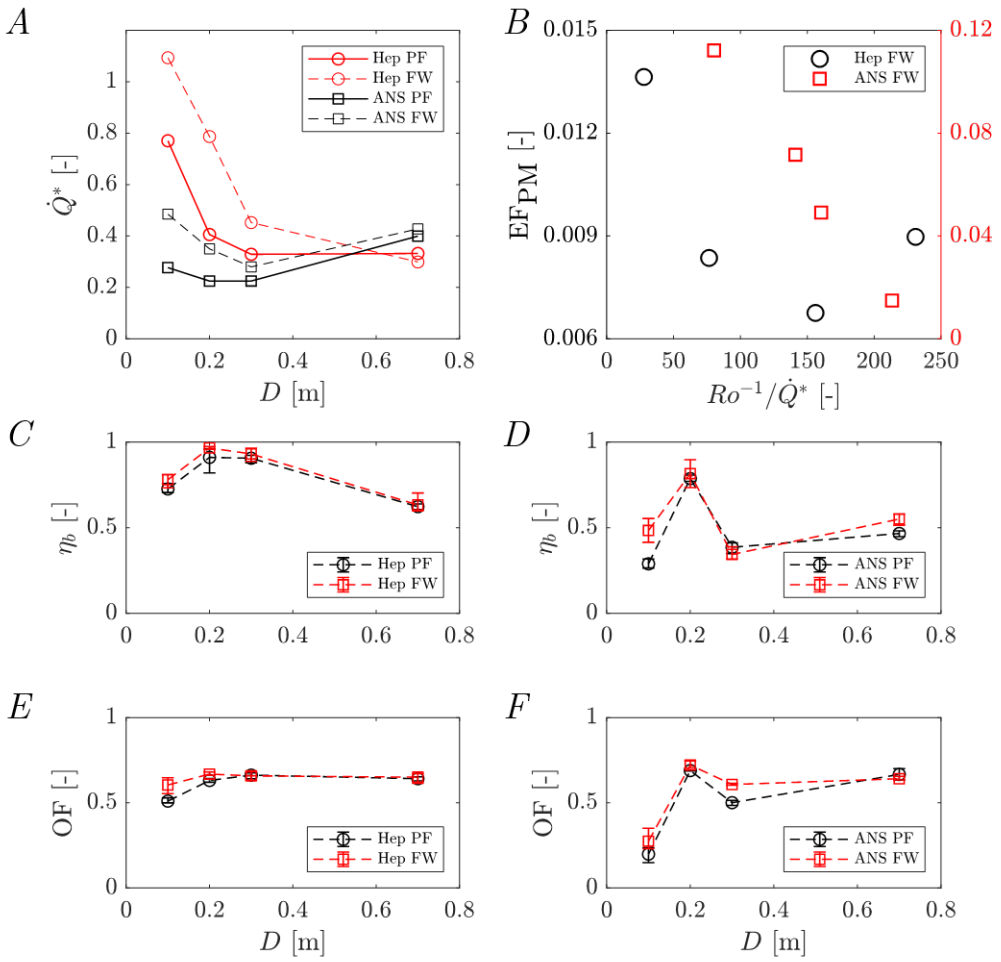

Figure 7: (A) Variation of $\dot{Q}^*$ with D. (B) Variation of $\mathrm{EF_{PM}}$ with $(Ro^{-1}/\dot{Q}^*)$. Burning efficiency for (C) heptane and (D) ANS fires. Oxidation factor for (E) heptane and (F) ANS fires.

a constant value of $\dot{Q}$, H_f first increases, then decreases. This change in H_f and w_f resulting from high Γ is referred to as "over-rotation" [45]. Above $(Ro^{-1}/\dot{Q}^*) \approx 150$, the increase in EF_{PM} may be attributed to over-rotation in heptane FWs. It appears that there may be a different value of this threshold for different fuels, since over-rotation was not observed for ANS FWs in Figure 7B.

For ANS FWs, the highest value of the ratio $(Ro^{-1}/\dot{Q}^*)$ is found at $D = 30$ cm. Going from $D = 30$ to $D = 70$ cm, the value of Ro^{-1} remains relatively unchanged (see Figure 3A), but $\dot{Q}^*$ increases (Figure 7A), causing $(Ro^{-1}/\dot{Q}^*)$ to decreases from 213 to 141. The increase in $\dot{Q}^*$ at 70 cm is a direct consequence of the steep rise in $\dot{m}''$ caused by boilover. In contrast, for heptane FWs, the largest value of the ratio $(Ro^{-1}/\dot{Q}^*)$ is 231, occurring at $D = 70$ cm. Similar to ANS FWs, heptane FWs at $D = [30, 70]$ cm have similar values for Ro^{-1}, but Figure 7A shows that heptane FWs have the lowest value of $\dot{Q}^*$ for fires at $D = 70$ cm. The significant reduction in $\dot{Q}^*$ from the $D = 30$ to 70 cm is the major contributing factor to increasing the effect of buoyancy (Figure 7B) on the FW and leads to an increase in the value of the ratio $Ro^{-1}/\dot{Q}^*$. Thus, over-rotation in heptane FWs at $D = 70$ cm is a consequence of a decline in $\dot{Q}^*$ rather than an increase in Ro^{-1}. It is hypothesized that if boilover did not occur, the value of $\dot{Q}^*$ would have been lower, causing the value of the ratio $(Ro^{-1}/\dot{Q}^*)$ at $D = 70$ cm to be higher than that at $D = 30$ cm, potentially presenting the opportunity for over-rotation to occur. This may not, however, be a preferred FW state for practical applications since it leads to an increase in EF_{PM}.

The variation of η_b and OF, calculated according to Equations 3 and 4, with D are shown in Figure 7 (C-E) for the all the different cases. Generally, FWs have higher values for both η_b and OF as compared to PFs, showing that a higher fraction of carbon from the fuel is oxidized to CO_2, causing EF_{PM} to be lower for FWs than for PFs. Based on the expressions in Equations 2 and 3, η_b is numerically equivalent to EF_{CO_2}. Again, the metrics η_b and OF are calculated based on gaseous components, which are primarily composed of CO_2. So even slight improvements in converting carbon in the fuel to CO_2 can result in significant reduction in soot (PM) emissions. Both these metrics are generally higher for heptane fires than for ANS fires.

4.2. Boilover

The violent burning of thin layers of oil over water is referred to as boilover [46]. Figure 8A shows a comparison of normal burning (panel A) and boilover burning (panel B). This regime of burning is caused by a sudden expansion of superheated water-vapor bubbles that nucleate at the fuel-water interface. Characteristics such as burning rate and flame height in this regime depend on many factors including slick thickness, D, fuel type and vaporization order, weathering, $\dot{q}''$, etc. [38, 47]. Generally, boilover causes a significant increase in both H_f and $\dot{m}$.

During boilover, the bubbles shoot through the fuel-water interface, ejecting oil droplets into the flame [46]. Streaks of these evaporating fuel droplets are visible in Figure 8B, significantly increasing the effective surface area for combustion. This results in the large value of both $\dot{m}''$ (Figure 2B) and η_{fuel} (Figure 2C) for ANS fires at the 70 cm scale when compared to the smaller scales. Boilover burning is also responsible for increased $\dot{q}''$ (Figure

3), partially through enhanced radiative feedback, which in turn sustains a high temperature at the fuel-water interface.

In this work, boilover was observed only with ANS crude oil, and was actively avoided in the $10 - 30$ cm experiments by using a magnetic stirrer to continuously mix the water sublayer. This ensured that the water bulk temperature increased only about $10 - 30$ K, depending on D and the flame regime. This prevented the fuel-water interface temperature from reaching boiling point, avoiding any bubble nucleation. At $D = 70$ cm, however, a stirrer could not be used. Instead, a recirculating pump system was installed to recirculate the water from the water-fuel interface to the bottom of the sublayer. The recirculation system, however, could not completely prevent boilover due to the large value of D, but could delay the onset. For ANS experiments at $D = 70$ cm, a slick thickness of 7 mm was used instead of the 5 mm that was used at the smaller scales. The recirculation system and increased slick thickness delayed boilover onset by about 40 s, allowing sufficient time for capturing data in both normal burning and boilover burning regimes.

The onset of boilover can be determined visually, but was also determined by the rate of emission of carbon emitted by the fire. This was determined from the cumulative measurements of the carbon emission from CO_2, CO and PM. Carbon-emission rate is almost constant during the normal burning, shown in Figure 8C for heptane PFs ($D = 70$ cm). When boilover occurs, however, the slope of this curve changes during the burning period, seen in Figure 8D, showing the carbon-emission rate for ANS PFs. The time at which the slope of the carbon-emission increases to a new value is denoted as the onset of boilover. For the 7 mm slicks used in these experiments, the mean boilover-onset time for PFs and FWs was 111 s and 63.5 s, respectively.

The carbon-emission rate is higher during the boilover phase because of the higher overall values of $\dot{m}$ and $\dot{m}''$ for ANS fires (Figure 2 A and B). The mass of fuel consumed in each phase was calculated using the boilover onset time, the fraction of O_2 consumed in the pre-boilover regime, and then extrapolating the fraction to the total fuel mass consumed. For FWs, only 14% of the fuel is burned prior to boilover onset, compared to 25% for PFs (Figure 8E). Thus, a majority of the fuel consumed by the FW is during the boilover phase, resulting in the steeper carbon-emission rate in Figure 8D.

Figure 4 and Table 2 show that the value of EF_{PM} for the pre- and post-boilover periods is very similar to the overall EF_{PM}, meaning that the fraction of total carbon in the fuel that is emitted as soot is similar in these periods. This suggests that in terms of soot emissions, the effectiveness of the FW regime is rather similar during normal burning and boilover burning. Present understanding of ISBs suggests that boilover does not occur over open water [5]. Given some of the benefits of boilover over normal burning such as increased $\dot{m}''$, η_b, radiative feedback, and an EF_{PM} similar to normal burning, it may be advantageous to purposely induce boilover in open-water ISBs.

4.3. Factors influencing PM emissions

There are differentiating factors between PFs and FWs and their relation to EF_{PM}. First, the higher oxygen consumption (and OF) for FWs suggests that their global equivalence ratio is leaner than that of PFs. This causes higher average temperatures in the FW structure,

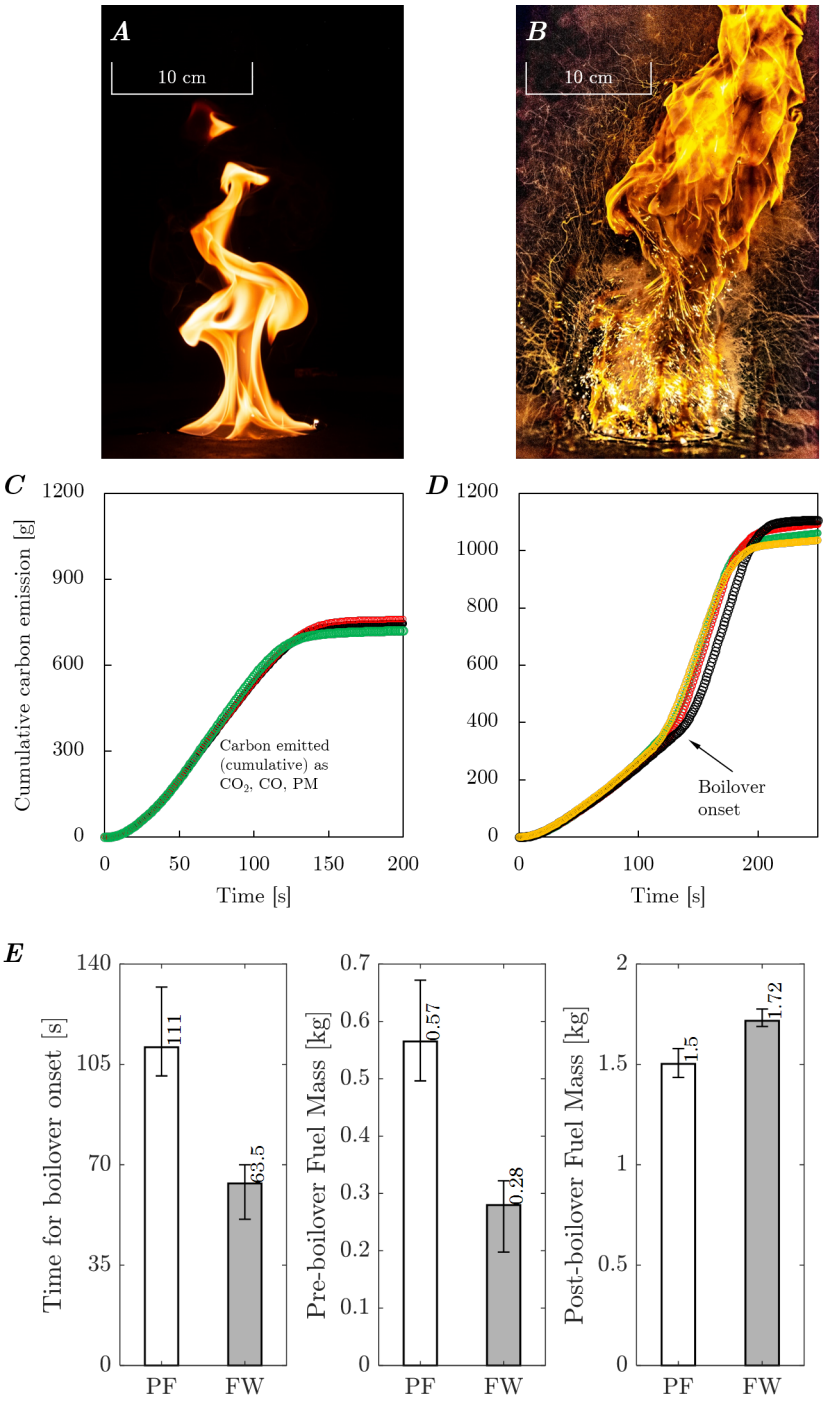

Figure 8: Images of a PF under (A) normal and (B) boilover burning, formed using a 5 mm slick of ANS crude oil at $D = 10$ cm. The streaks seen in (B) are formed by the fuel droplets emanating from the fuel pool. Variation of carbon-emission rate with time ($D = 70$ cm) for (C) heptane PF and (D) ANS PF. (E) Bar graphs showing the difference between PFs and FWs ($D = 70$ cm) on the basis of time for onset of boilover, fuel mass consumed before boilover onset, and fuel mass consumed during boilover.

which has a larger surface area as compared to PFs. The high temperatures and improved view factor results in higher radiative heat feedback to the fuel pool [36]. The radiative feedback is higher in ANS fires than heptane fires (Figure 3) due to the higher concentration of soot particles in the flame. The convective heat feedback is also enhanced by the strong radial inflow at the bottom boundary layer [26]. When compared to PFs, increased heat feedback ($\dot{q}''$) leads to higher fuel-evaporation rate ($\dot{m}$) and thus, higher heat-release rates ($\dot{Q}$). In a FW apparatus with natural air entrainment, increased $\dot{Q}$ corresponds to increased U_θ and Γ, which in turn contribute to decreasing overall equivalence ratio, increasing OF, ΔT and $\dot{q}''$, completing the feedback loop. The increase in q_f^* with Γ, and the higher η_{fuel} values for ANS FWs indicate that the high-molecular-weight components in ANS crude oil require higher heat feedback to evaporate [47]. Overall, the lower $\mathrm{EF_{PM}}$ from FWs is a consequence of higher burning efficiency as compared to PFs.

The exact mechanisms leading to a reduction of $\mathrm{EF_{PM}}$ when a pool of fuel is burned as a FW rather than a PF are not immediately apparent from the data presented here. The complex feedback mechanism between the fluid dynamics of air entrainment and combustion in the whirling flames needs to be investigated further. More detailed experiments at small length scales will shed light on the role of the vortex structure, turbulence and mixing characteristics, and their interplay with the chemical kinetics of soot formation and destruction. Additionally, the effects of boilover are not fully understood in the context of emissions and is dependent on the flame regime. For instance, considering $\mathrm{EF_{CO}}$ from PFs, post-boilover emissions are higher than pre-boilover, but this is reversed for FWs. Still, boilover has only a minimal effect on the overall $\mathrm{EF_{PM}}$. The data presented here serves as a platform for more detailed investigations in the future by incorporating the effects of chemical kinetics and soot formation using a combination of non-intrusive diagnostics, scaling methods and numerical simulations.

5. Summary and Conclusions

An experimental investigation of airborne emissions from pool fires and fire whirls was conducted at fuel-pool diameters of 10, 20, 30 and 70 cm. Two liquid fuels were used, heptane and ANS crude oil. Free-buoyant pool fires were formed in a quiescent background, and fire whirls were formed in a fixed-frame setup that allowed natural entrainment of air. Attributes such as burning rate, burning efficiency, emissions of particulate matter, carbon dioxide, carbon monoxide, and oxygen consumption were measured for the different pool diameters and flame regimes. Results showed that for both fuels, as compared to pool fires, fire whirls burned fuel at higher rates. When burning ANS crude oil, the mass of unburned residue was lower for fire whirls, showing that the fuel consumption efficiency of fire whirls was also higher.

Although the burning rate was higher for fire whirls, the peak emission rate of particulate matter (soot) form fire whirls was lower than from pool fires. The emission factor of particulate matter emissions from fire whirls was $\sim 50\%$ lower than that from pool fires. This was true for both heptane and ANS crude oil, across all pool diameters. For pool fires and fire whirls, the emissions behavior of the two fuels was significantly different. The

emission factor of particulate matter for ANS crude oil fires was an order magnitude higher than that for heptane fires. The burning efficiency also showed that over half of the carbon in the crude oil was emitted as unburned hydrocarbons. This is attributed to the significant differences in the composition of the fuels and the fires they supported.

For the fire whirls in the study, a ratio of the inverse of the Rossby number and nondimensional heat-release rate, $Ro^{-1}/\dot{Q}^*$, was defined to compare the effects of buoyancy and circulation on the fire. As the value of $Ro^{-1}/\dot{Q}^*$ increased, the emission factor of particulate matter decreased linearly for ANS fire whirls. For heptane fire whirls, the linear relationship existed for diameters between 10 and 30 cm, but increased at 70 cm. Generally, the flame height of a fire whirl increases with Ro^{-1}. But beyond an upper threshold, the flame height reduces and flame width increases. This is a state referred to as over-rotation, which also corresponds to an increase in particulate emissions. While over-rotation has been reported qualitatively in the literature [44, 45], the ratio $Ro^{-1}/\dot{Q}^*$ quantifies the phenomenon and helps explain the increase in emissions as a consequence of the decrease in flame surface area.

Over-rotation was not observed in fire whirls formed using ANS crude oil at the 70 cm scale. This is attributed to another phenomenon, boilover, which occurs during burning of thin films of dense hydrocarbons floating over a water surface. Boilover caused a rapid increase in burning rate, which resulted in an increase in heat-release rate and buoyancy. This was reflected in a significant decrease in the ratio $Ro^{-1}/\dot{Q}^*$, corresponding to an increase in the buoyant momentum relative to tangential momentum. Boilover ensured that over-rotation did not occur. The high burning rate during boilover also resulted in significant increases in the flame height and fuel-consumption efficiency. The onset time of boilover was lower for fire whirls, and fire whirls also consumed a higher fraction of the initial fuel mass during the boilover period. Additionally, the overall particulate-matter emission factor was similar to that in the pre-boilover and post-boilover periods, showing that it may be advantageous to induce boilover during *in-situ* burns.

The reduction in particulate-matter emissions from fire whirls is attributed to the following factors. Compared to pool fires, fire whirls consume more oxygen per unit mass of fuel, leading to a lower global equivalence ratio. They also have higher burning efficiency, and a higher fraction of the oxygen consumed was converted to carbon dioxide. Collectively, these result in higher temperatures in the fire whirl structure, leading to the higher heat feedback to the fuel surface. Heat feedback increased linearly with pool diameter and circulation, and led to higher burning rate, which in turn resulted in higher air-entrainment velocities, which in turn leads to higher oxygen supply to the fire whirl, completing the feedback loop.

A number of open questions regarding the emissions from fire whirls remain to be answered before practical applications are considered. While soot-free whirling flames such as the "blue whirl" are known in the literature [48, 49, 50], they form at very small length scales [40] and the transition to the blue whirl is highly sensitive to experimental conditions [51, 52]. Fire whirls, on the other hand, can be formed more robustly across a large range of length scales. While fire whirls do emit some quantities of soot, the results of this work demonstrate that they can still offer opportunities to significantly reduce the environmental impact of ISBs, which are currently burned as pool fires [53]. The range of heat-release rates and

circulations for fire whirls in this study is wider than those in the literature, although these factors were not varied independently in this study and only the natural-entrainment configuration was used. To understand the independent effect of these parameters on emissions, systematically varying these quantities by controlling air entrainment could help isolate the effects. The effect of boilover on emissions needs to be investigated further since its onset does not seem to significantly affect the particulate-matter emission factor. The metrics presented here provide a global explanation for the reduction in particulate emissions compared to pool fires, and future work will focus on the exact mechanisms leading to efficient combustion.

6. Acknowledgements

The authors thank the Bureau of Safety and Environmental Enforcement (BSEE, contract no. E17PC00016) for supporting this work, Program Manager Karen Stone for significant guidance and suggestions. The authors also thank Dr. Ali Tohidi, Dr. Yu Hu, Michael Jones at the Department of Fire Protection Engineering, UMD, and Raymond T. Ranellone, Chris D. Nelson, Fredrick M. Brokaw and Nate Saur at the WPI Fire Protection Engineering Performance Laboratory for assistance with experiments.

7. Declaration of interests

The authors declare that they have no known competing financial interests or personal relationships that could have appeared to influence the work reported in this paper.

References

[1] G. M. Solomon, S. Janssen, Health effects of the gulf oil spill, Disaster Medicine and Public Health Preparedness 4 (2010) 273–276.

[2] J. P. Zock, G. Rodríguez-Trigo, F. Pozo-Rodríguez, J. A. Barberà, L. Bouso, Y. Torralba, J. M. Antó, F. P. Gómez, C. Fuster, H. Verea, Prolonged respiratory symptoms in clean-up workers of the Prestige oil spill, American Journal of Respiratory and Critical Care Medicine 176 (2007) 610–616.

[3] C. H. Peterson, S. D. Rice, J. W. Short, D. Esler, J. L. Bodkin, B. E. Ballachey, D. B. Irons, Long-Term Ecosystem Response to the Exxon Valdez Oil Spill, Science 302 (2003) 2082–2086.

[4] J. M. Teal, R. W. Howarth, Oil spill studies: A review of ecological effects, Environmental Management 8 (1984) 27–43.

[5] M. F. Fingas, G. Halley, F. Ackerman, R. Nelson, M. Bissonnette, N. Laroche, Z. Wang, P. Lambert, K. Li, P. Jokuty, G. Sergy, E. J. Tennyson, J. Mullin, L. Hannon, W. Halley, J. Latour, R. Galarneau, B. Ryan, R. Turpin, P. Campagna, D. V. Aurand, R. R. Hiltabrand, The Newfoundland Offshore Burn Experiment—NOBE, International Oil Spill Conference Proceedings 1995 (1995) 123–132.

[6] J. L. Ross, R. J. Ferek, P. V. Hobbs, Particle and Gas Emissions from an In Situ Burn of Crude Oil on the Ocean, Journal of the Air & Waste Management Association 46 (1996) 251–259.

[7] A. A. Allen, R. J. Ferek, Advantages and Disadvantages of Burning Spilled Oil, International Oil Spill Conference Proceedings 1993 (1993) 765–772.

[8] I. Buist, K. Trudel, J. Morrison, D. Aurand, Laboratory Studies of the Properties of In-Situ Burn Residues, International Oil Spill Conference Proceedings 1997 (1997) 149–156.

[9] Q. Lin, I. A. Mendelssohn, K. Carney, S. M. Miles, N. P. Bryner, W. D. Walton, In-situ burning of oil in coastal marshes. 2. Oil spill cleanup efficiency as a function of oil type, marsh type, and water depth, Environmental Science and Technology 39 (2005) 1855–1860.

[10] I. Buist, Window-of-opportunity for in situ burning, Spill Science and Technology Bulletin 8 (2003) 341–346.
[11] J. Aurell, B. K. Gullett, D. Yamamoto, Emissions from Open Burning of Simulated Military Waste from Forward Operating Bases, Environmental Science & Technology 46 (2012) 11004–11012.
[12] J. Aurell, D. Hubble, B. K. Gullett, A. Holder, E. Washburn, D. Tabor, Characterization of Emissions from Liquid Fuel and Propane Open Burns, Fire Technology 53 (2017) 2023–2038.
[13] S. P. Urbanski, Combustion efficiency and emission factors for wildfire-season fires in mixed conifer forests of the northern Rocky Mountains, US, Atmospheric Chemistry and Physics 13 (2013) 7241–7262.
[14] R. J. Yokelson, S. P. Urbanski, E. L. Atlas, D. W. Toohey, E. C. Alvarado, J. D. Crounse, P. O. Wennberg, M. E. Fisher, C. E. Wold, T. L. Campos, K. Adachi, P. R. Buseck, W. M. Hao, Emissions from forest fires near Mexico City, Atmospheric Chemistry and Physics 7 (2007) 5569–5584.
[15] N. May, E. Ellicott, M. Gollner, An examination of fuel moisture, energy release and emissions during laboratory burning of live wildland fuels, International Journal of Wildland Fire 28 (2019) 187–197.
[16] National-Response-Team, Guidance on Burning Spilled Oil in Situ, Technical Report December 1995, Office of Response and Restoration, 1995.
[17] IPIECA, IOGP, In-Situ Burning of Spilled Oil - Good practice guidelines for incident management and emergency response personnel, Technical Report, IPIECA, IOGP, London, UK, 2016.
[18] ExxonMobil, Alaska North Slope Material Safety Data Sheet, 2018.
[19] I. Glassman, Soot formation in combustion processes, Symposium (International) on Combustion 22 (1989) 295–311.
[20] N. Syred, J. Beér, Combustion in swirling flows: A review, Combustion and Flame 23 (1974) 143–201.
[21] R. A. Yetter, I. Glassman, H. C. Gabler, Asymmetric Whirl Combustion: A New Low NOx Approach, Proceedings of the Combustion Institute 28 (2000) 1265–1272.
[22] S. Candel, D. Durox, T. Schuller, J.-F. Bourgouin, J. P. Moeck, Dynamics of Swirling Flames, Annual Review of Fluid Mechanics 46 (2014) 147–173.
[23] H. W. Emmons, S.-J. Ying, The fire whirl, Symposium (International) on Combustion 11 (1967) 475–488.
[24] P. Wang, N. Liu, K. Hartl, A. Smits, Measurement of the Flow Field of Fire Whirl, Fire Technology 52 (2016) 263–272.
[25] J. Lei, N. Liu, R. Tu, Flame height of turbulent fire whirls: A model study by concept of turbulence suppression, Proceedings of the Combustion Institute 36 (2017) 3131–3138.
[26] J. Lei, N. Liu, L. Zhang, Z. Deng, N. K. Akafuah, T. Li, K. Saito, K. Satoh, Burning rates of liquid fuels in fire whirls, Combustion and Flame 159 (2012) 2104–2114.
[27] G. M. Byram, R. E. Martin, Fire Whirlwinds in the Laboratory, Fire Control Notes 23 (1962) 13–17.
[28] T. Incorporated, Theory of Operation - DustTrak DRX Aerosol Monitor, Technical Report, TSI Incorporated, 2012.
[29] R. J. Yokelson, J. G. Goode, D. E. Ward, R. A. Susott, R. E. Babbitt, D. D. Wade, I. Bertschi, D. W. T. Griffith, W. M. Hao, Emissions of formaldehyde, acetic acid, methanol, and other trace gases from biomass fires in North Carolina measured by airborne Fourier transform infrared spectroscopy, Journal of Geophysical Research: Atmospheres 104 (1999) 30109–30125.
[30] L. Hu, J. Hu, J. L. de Ris, Flame necking-in and instability characterization in small and medium pool fires with different lip heights, Combustion and Flame 162 (2015) 1095–1103.
[31] A. Hamins, J. Yang, T. Kashiwagi, An experimental investigation of the pulsation frequency of flames, Symposium (International) on Combustion 24 (1992) 1695–1702.
[32] W. Coenen, E. J. Kolb, A. L. Sánchez, F. A. Williams, Observed dependence of characteristics of liquid-pool fires on swirl magnitude, Combustion and Flame 205 (2019) 1–6.
[33] J. Lei, N. Liu, Y. Jiao, S. Zhang, Experimental investigation on flame patterns of buoyant diffusion flame in a large range of imposed circulations, Proceedings of the Combustion Institute 36 (2017) 3149–3156.
[34] K. H. Chuah, K. Kuwana, K. Saito, F. A. Williams, Inclined fire whirls, Proceedings of the Combustion Institute 33 (2011) 2417–2424.

[35] W. Tang, C. H. Miller, M. J. Gollner, Local flame attachment and heat fluxes in wind-driven line fires, Proceedings of the Combustion Institute 36 (2017) 3253–3261.
[36] R. Dobashi, T. Okura, R. Nagaoka, Y. Hayashi, T. Mogi, Experimental Study on Flame Height and Radiant Heat of Fire Whirls, Fire Technology 52 (2016) 1069–1080.
[37] K. Zhou, N. Liu, J. S. Lozano, Y. Shan, B. Yao, K. Satoh, Effect of flow circulation on combustion dynamics of fire whirl, Proceedings of the Combustion Institute 34 (2013) 2617–2624.
[38] L. van Gelderen, G. Jomaas, The Parameters Controlling the Burning Efficiency of In-Situ Burning of Crude Oil on Water, in: Proceedings of the 40th AMOP Technical Seminar on Environmental Contamination and Response, Calgary, Canada, pp. 817–832.
[39] K. Noto, K. Teramoto, T. Nakajima, Spectra and critical grashof numbers for turbulent transition in a thermal plume, Journal of Thermophysics and Heat Transfer 13 (1999) 82–90.
[40] Y. Hu, S. B. Hariharan, H. Qi, M. J. Gollner, E. S. Oran, Conditions for formation of the blue whirl, Combustion and Flame 205 (2019) 147–153.
[41] J. Lei, C. Ji, N. Liu, L. Zhang, Effect of imposed circulation on temperature and velocity in general fire whirl: An experimental investigation, Proceedings of the Combustion Institute 37 (2019) 4295–4302.
[42] A. Tohidi, M. J. Gollner, H. Xiao, Fire Whirls, Annual Review of Fluid Mechanics 50 (2018) 187–213.
[43] S. R. Turns, An Introduction to Combustion: Concepts and Applications, McGraw-Hill, 3rd edition, 2012.
[44] N. Chigier, J. Beér, D. Grecov, K. Bassindale, Jet flames in rotating flow fields, Combustion and Flame 14 (1970) 171–179.
[45] R. ZHOU, Z.-N. WU, Fire whirls due to surrounding flame sources and the influence of the rotation speed on the flame height, Journal of Fluid Mechanics 583 (2007) 313–345.
[46] J. P. Garo, J. P. Vantelon, A. C. Fernandez-Pello, Boilover burning of oil spilled on water, Symposium (International) on Combustion 25 (1994) 1481–1488.
[47] L. V. Gelderen, L. M. V. Malmquist, G. Jomaas, Vaporization order and burning efficiency of crude oils during in - situ burning on water, Fuel 191 (2017) 528–537.
[48] S. B. Hariharan, E. T. Sluder, M. J. Gollner, E. S. Oran, Thermal structure of the blue whirl, Proceedings of the Combustion Institute 37 (2019) 4285–4293.
[49] S. B. Hariharan, The Structure of the Blue Whirl: A Soot-Free Reacting Vortex Phenomenon, Ph.D. thesis, University of Maryland, College Park, 2017.
[50] S. B. Hariharan, Experimental Investigations and Scaling Analyses of Whirling Flames, Ph.D. thesis, University of Maryland, College Park, 2020.
[51] S. B. Hariharan, P. M. Anderson, H. Xiao, M. J. Gollner, E. S. Oran, The blue whirl: Boundary layer effects, temperature and OH* measurements, Combustion and Flame 203 (2019) 352–361.
[52] S. B. Hariharan, Y. Hu, M. J. Gollner, E. S. Oran, Effects of circulation and buoyancy on the transition from a fire whirl to a blue whirl, Physical Review Fluids 5 (2020) 103201.
[53] M. J. Gollner, E. S. Oran, S. B. Hariharan, J. Dowling, H. F. Farahani, A. S. Rangwala, Efficient Remediation of Oil Spills over Water using Fire Whirls (Project Number 1094), Technical Report, Bureau of Safety and Environmental Enforcement, Washington, DC, 2019.